



Performance of non-porous graphite and titanium-based anodes in microbial fuel cells

Annemiek ter Heijne^{a,b}, Hubertus V.M. Hamelers^{a,*}, Michel Saakes^b, Cees J.N. Buisman^{a,b}

^a Sub-Department of Environmental Technology, Wageningen University, Bomenweg 2, P.O. Box 8129, 6700 EV Wageningen, The Netherlands

^b Wetsus, Centre of Excellence for Sustainable Water Technology, Agora 1, P.O. Box 1113, 8900 CC Leeuwarden, The Netherlands

ARTICLE INFO

Article history:

Received 26 November 2007

Received in revised form 10 March 2008

Accepted 15 March 2008

Available online 22 March 2008

Keywords:

Microbial fuel cell

Anode

Graphite

Titanium

Impedance spectroscopy

ABSTRACT

Four non-porous materials were compared for their suitability as bio-anode in microbial fuel cells (MFCs). These materials were flat graphite, roughened graphite, Pt-coated titanium, and uncoated titanium. The materials were placed in four identical MFCs, of which the anode compartments were hydraulically connected in series, as well as the cathode compartments. The MFCs were operated with four resistors. The anode kinetics at these electrode materials were studied by means of dc-voltammetry and electrochemical impedance spectroscopy (EIS). Both techniques were compared and showed that the bio-anode performance decreased in the order roughened graphite > Pt-coated titanium > flat graphite > uncoated titanium. Uncoated titanium was unsuitable as anode material. For the other three materials, specific surface area was not the single variable explaining the differences in current density for the different materials. All polarization curves showed a clear limiting current. This limit could not be attributed to mass transfer of the substrate and reflected the maximum biomass activity. The current density of the non-porous bio-anodes, except for the uncoated titanium anode, was comparable to the reported current densities of porous materials when normalized to the projected surface area. The high current densities that were recorded by dc-voltammetry, however, could not be maintained in a stable way for a longer period. This shows that polarization curves of MFCs should be evaluated critically.

© 2008 Elsevier Ltd. All rights reserved.

1. Introduction

The microbial fuel cell (MFC) is a promising technology to convert biodegradable materials, e.g. organic materials present in wastewater, into electricity. The technology is based on electrochemically active microorganisms that grow by oxidizing the biodegradable material to CO₂ and protons while transferring the electrons to a solid electrode [1]. Electron transfer from the microorganisms to the electrode can occur via several mechanisms [2,3]. When using a mixed culture in a system with continuous flow, it is likely that the current is produced by a thin biofilm attached to the surface of the electrode, as the electrochemically active microorganisms close to the electrode have a competitive advantage.

The power output of the MFC is amongst others influenced by the electrochemical performance of the bio-anode. The bio-anode is defined here as the assembly of the biofilm and the solid electrode to which it is attached. The electrochemical performance of the bio-anode can be expressed in a polarization curve, i.e. the relationship between the current density and the anode potential. Two main

processes can be distinguished that influence the polarization curve of the bio-anode: (i) the microbial kinetics of substrate oxidation and the associated electron transfer and (ii) the mass transfer of substrate and products. To study the microbial kinetics of the bio-anode, a polarization curve can only be useful if mass transfer is not determining the current density. The effect of mass transfer on the current density can be eliminated or decreased by proper design of the MFC, such that the bio-anode has a thin diffusion layer.

Until now, mainly porous carbon-based materials, like graphite felt, graphite granules, carbon cloth, and reticulated vitreous carbon (RVC, porous glassy carbon) have been used as anodes [4–7]. Carbon-based materials are attractive because they are relatively cheap. Porous materials are of major practical importance because they have a high specific surface area which is expected to lead to high volumetric activity. To study specific materials, however, a non-porous electrode is beneficial because mass transfer can be quantified. For porous materials on the other hand, mass transfer is difficult to quantify, because of the unknown thickness of the diffusion layer. This unknown mass transfer makes interpretation of measurement data for porous materials more difficult. Platinum has been tested as anode material in MFCs because of its catalytic activity for hydrogen oxidation [8,9].

* Corresponding author. Tel.: +31 317 483447; fax: +31 317 482108.

E-mail address: Bert.Hamelers@wur.nl (H.V.M. Hamelers).

An electrode material needs to have certain properties to be suitable as a bio-anode: it should (i) have good bio-compatibility to support microbial growth, (ii) have high electrical conductivity, and (iii) be electrochemically inert [10]. Based on the properties mentioned above, four electrode materials were selected: flat graphite, roughened graphite, Pt-coated titanium, and uncoated titanium. The objective of this study was to study the bio-anode kinetics at these non-porous electrode materials. The materials were placed in four identical MFCs, of which the anode compartments were hydraulically connected in series to ensure an equal anolyte composition, including dispersed biomass. The microbial kinetics were studied by means of dc-voltammetry and electrochemical impedance spectroscopy (EIS).

2. Experimental

2.1. Microbial fuel cell design and setup

The experimental setup consisted of four identical MFCs. All four anode compartments were hydraulically connected in series, as well as all four cathode compartments. Each MFC consisted of two plexiglass plates with a single flow channel, two electrodes, and two plexiglass support plates (Fig. 1). The two plates with a flow channel were separated by a cation exchange membrane (Fumasep FKB, Fumatech, St. Ingbert, Germany). The other side of the flow channel faced the electrode.

The anodes were made of four different materials: flat graphite, Al₂O₃-blasted graphite (further called: roughened graphite) (both MR200, gas tight impregnated, from Müller & Rössner GmbH & Co., Troisdorf, Germany), Pt-coated titanium, and uncoated titanium (both from Magneto Special Anodes BV, Schiedam, The Netherlands). Although Pt-coated titanium has electrochemical catalytic activity, for e.g. oxidation of hydrogen gas to protons, initial experiments showed that Pt-coated titanium had no catalytic activity for oxidation of acetate. All four cathodes were flat graphite plates (Müller & Rössner GmbH & Co., Troisdorf, Germany). The surface area of the flow channel, and thus the projected surface area of the electrodes in contact with solution, was 22 cm², and the volume of the flow channel was 33 mL (11.2 cm length × 2.0 cm width × 1.5 cm height).

2.2. Microbial fuel cell operation

The anolyte was inoculated with the effluent of another MFC run on acetate [11]. Both anode and cathode compartments were equipped with Ag/AgCl, 3 M KCl reference electrodes (+205 mV vs. NHE). Potentials of anode vs. reference electrode and cell voltages of each MFC were collected every 60 s via a Fieldpoint FP-AI-110 module connected to a PC. The MFCs were operated in a temperature controlled chamber at 30 °C.

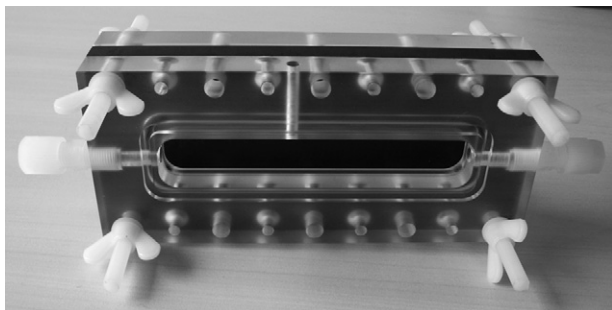


Fig. 1. MFC design: the assembly of flow channel, flat graphite electrode, and support plate of one side of the MFC.

The MFCs were each started with a resistance of 1000 Ω and with a 0.020 M phosphate buffer at pH 7 in the cathode. After two weeks of operation, the catholyte was replaced with a Fe(III)[CN]₆³⁻ solution (0.050 M) in 0.020 M buffer (pH 7) for a fast cathode reaction (reduction of Fe(III)[CN]₆³⁻ to Fe(II)[CN]₆⁴⁻). Four resistors with a range of 0–1000 Ω were used. Fresh anolyte, consisting of 0.020 M potassium acetate solution in 0.020 M phosphate buffer at pH 7, was fed at a rate of 0.15 L/d. Anolyte pH was controlled at 7. Anolyte and catholyte were recirculated at a flow rate of 10 L/h.

The MFCs were operated at three different resistances with Fe(III)[CN]₆³⁻ in the cathode: first $R = 1000 \Omega$ during 9 days, second $R = 250 \Omega$ during 5 days, and third $R = 100 \Omega$ during 6 days, except for the MFC with the uncoated titanium anode, which was operated with a resistance of 500 Ω instead of 250 Ω for 5 days, and was changed back to $R = 1000 \Omega$ due to its bad performance (anode potential > +100 mV vs. Ag/AgCl). At the end of each period, when anode potential was stable (difference in anode potential between two days < 10 mV, and daily standard deviations < 10 mV), each MFC was characterized with a potentiostat (IVIUMStat, Ivium Technologies, Eindhoven, The Netherlands) by EIS and dc-voltammetry. After the third resistance ($R = 100 \Omega$), anode potential did not become stable. To be able to measure at a stable situation, the resistor was increased to $R = 250 \Omega$ for 16 h before EIS and dc-voltammetry measurements, was kept at 250 Ω during the following 7 days, and was finally increased to $R = 1000 \Omega$ during 6 days.

The anolyte was supplied with nutrients and vitamins in batch. At the start, and after each change in resistance, the following solutions were supplied to the anolyte: 10 mL/L of a macronutrient solution containing 28 g/L NH₄Cl, 10 g/L MgSO₄·7H₂O, and 0.57 g/L CaCl₂·2H₂O, 2 mL/L of a micronutrient solution containing 2 g/L FeCl₂·4H₂O, 1 g/L CoCl₂·6H₂O, 0.5 g/L MnCl₂·4H₂O, 0.05 g/L ZnCl₂, 0.05 g/L H₃BO₃, 0.04 g/L CuCl₂·2H₂O, 0.07 g/L (NH₄)₆Mo₇O₂₄·5H₂O, 1 g/L NiCl₂·6H₂O, 0.16 g/L Na₂SeO₃·5H₂O and 2 mL/L 37% HCl (adapted from [12]), and 1 mL/L of a vitamin solution as described in [11].

Samples were taken from the anode each time that a measurement was performed and were analyzed for their acetate concentrations.

2.3. Measurements and data analysis

Current density I (A/m²) was calculated from the cell voltage E (V), the resistance R (Ω) and the projected electrode surface area A_{el} (m²) according to $I = \frac{E}{RA_{el}}$. Average current density, average anode potential, and their standard deviations were calculated over 24 h from data obtained every 60 s. Polarization curves were obtained by dc-voltammetry, using the method chronoamperometry. The cell voltage was decreased stepwise and was kept at each voltage for 120 s in order to let the dc-current stabilize. The MFCs were measured in the range of 0.65–0.30 V (cell voltage) in steps of 0.050 V, except for MFC with the uncoated titanium anode, which was measured in the range of 0.3–0.1 V (cell voltage). The last data point at each voltage, after 120 s, was selected for data presentation. Anode potential was measured every 30 s during these measurements on a PC via the Fieldpoint module.

Impedance was measured at 22 frequencies between 40–0.003 Hz. The cell voltage at which the impedance measurement was performed was the cell voltage of the MFC when operated with the resistor, for both $R = 1000 \Omega$ and $R = 250 \Omega$. As anode potential did not become stable at $R = 100 \Omega$, impedance was measured at the same cell voltage as before with $R = 250 \Omega$. Each MFC was pretreated for 300 s at this cell voltage before impedance measurement was started, so the MFC was stable at the start of the measurement.

The equivalent circuit to which the data were fitted consisted of a constant phase element (CPE) [13] and a charge transfer resis-

tance (R_{ct}) in parallel (representing the anode), placed in series with a solution resistance R_s . The impedance of the CPE was described by $Z = \frac{1}{CPE^\alpha}$ where Z = magnitude of the impedance (Ω), and α = roughness factor (-). The equivalent circuit fitting was done by a program written in Mathcad. Four parameters were fitted: CPE, α , charge transfer resistance and solution resistance. The capacitance was calculated from the CPE and α according to [14]: $C = CPE \cdot (\omega_{max})^{(\alpha-1)}$ where C = capacitance (F), and ω_{max} = angular frequency at which the maximum R_{lm} is obtained (rad/s).

Acetate concentrations were determined using a Gas Chromatograph (GC). The GC (HP 5890 series II, Agilent Technologies, Amstelveen, The Netherlands) was equipped with an AT-Aquawax-DA column (Alltech) and a flame ionization detector (FID). Temperature was raised from 80 °C to 210 °C, at 25 °C/min. Nitrogen was used as carrier gas.

Biomass density could not be determined, because we performed consecutive runs in between which the MFCs could not be disassembled. We report the dependence of current on anode potential to show the microbial kinetics at different anode materials. The use of $Fe(III)[CN]_6^{3-}$ as an electron acceptor is convenient when studying the anode kinetics, however, $Fe(III)[CN]_6^{3-}$ is not suitable for practical application because it cannot be regenerated without external energy input. Cell voltage and power density are therefore not shown.

2.4. Mass transfer calculations

As non-porous electrodes are used, it may be safely assumed that the mass transfer is determined by the stagnant water layer attached to the electrode. This stagnant water layer is the result of the biofilm that holds water, and the hydrodynamic boundary layer. Biofilms observed so far in MFCs are thin, ranging from a monolayer [15] to maximally about 40 μm [16]. The thickness of the hydrodynamic boundary layer was calculated to be 155 μm (see below), and therefore, we assume that this hydrodynamic boundary layer, and not the biofilm, mainly determined the effect of mass transfer on the current density. The average mass transfer rate in the reactor for laminar flow can be calculated using [17]:

$$Sh = 3.66 \left(1 + 0.095 \frac{D_T}{L} Pe \right)^{0.45}$$

$$Pe = \frac{D_T v}{D}$$

$$Sh = \frac{k D_T}{D}$$

$$\delta = \frac{D}{k}$$

where Sh = Sherwood number (-), D_T = hydraulic diameter (m) = $\frac{2WH}{W+H}$ (with W = width = 2.0 cm, H = height = 1.5 cm), L = channel length = 12 cm, Pe = Peclet number (-), v = flow velocity = 1.0 cm/s, D = diffusion coefficient for acetate = $1.2 \times 10^{-9} m^2/s$ [18], k = mass transfer coefficient (m/s), and δ = thickness of the hydrodynamic boundary layer (m).

The flow was calculated to be laminar using the Reynolds number: $Re = \frac{D_T v \rho}{\mu} = 193$, where ρ = density = $1 \times 10^3 kg/m^3$, and μ = viscosity = $8.9 \times 10^{-4} Pa/s$.

The mass transfer coefficient was calculated to be $k = 7.7 \times 10^{-6} m/s$, and thus the thickness of the hydrodynamic boundary layer was 155 μm .

When the substrate at the electrode surface is depleted, the maximum mass transfer rate is observed. Under these conditions a limiting current density, (I_l , A/m^2) is observed, which can be

calculated as: $I_l = n F k c^*$ [19], where $n=8$ (number of electrons per acetate), F = Faraday's constant (96485 C/mol), and c^* = bulk acetate concentration (mol/m³). The resulting limiting current density is for example 39 A/m^2 at an acetate concentration of $6.5 \times 10^{-3} M$.

2.5. Specific surface area (Atomic Force Microscopy)

The specific surface area of the electrode materials was determined with an Atomic Force Microscope (NanoScope IIIa, Veeco, Santa Barbara, California). To determine the specific surface area on relevant scales, we have studied the surfaces on the scale of the biofilm (20 $\mu m \times 20 \mu m$) and on the scale of a microorganism (2 $\mu m \times 2 \mu m$). The resolution used was between 512 \times 256 and 512 \times 512, depending on the roughness of the sample. The specific surface area was calculated as the actual surface area (μm^2) divided by the projected surface area (μm^2), and was thereafter normalized to the surface area of the flat graphite electrode.

3. Results and discussion

3.1. Overall performance of the bio-anodes

The average daily current densities with standard deviations of the four anodes in time are shown in Fig. 2A. The average daily anode potential and the standard deviations of flat graphite, roughened graphite, and Pt-coated titanium are shown in Fig. 2B. The anodes based on flat graphite, roughened graphite, and Pt-coated titanium operated steady at 1000 Ω (day 0–8) and at 250 Ω (day

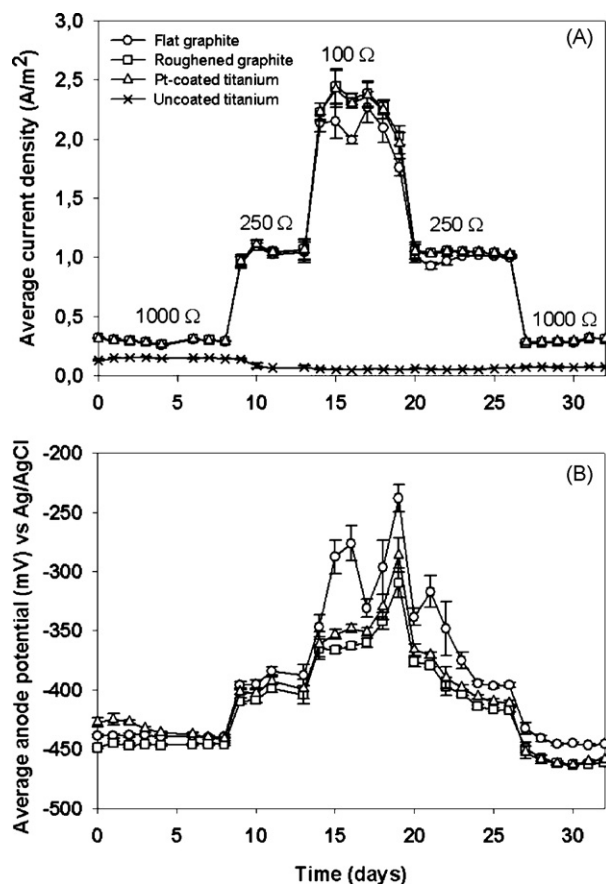


Fig. 2. (A) Average daily current production (A/m^2 , normalized to the projected surface area) of the four anodes. (B) Average daily anode potential (mV) vs. Ag/AgCl of the roughened graphite, Pt-coated titanium, and flat graphite electrode.

9–13), however, they did not reach a stable potential and current when operated at 100 Ω (day 14–19). At this resistance, we observed high variations in the daily current density and anode potential, and the performance decreased considerably during the last two days of operation at this resistance. The Pt-coated titanium, roughened graphite, and flat graphite anodes changed to steady operation again after the resistors were increased to 250 Ω (day 20–26), and to 1000 Ω (day 27–32), and the produced current was similar to the current at that same resistance before. The anode potential was similar to the anode potential at the same resistance before as well. The uncoated titanium anode had the lowest current. This current did not increase as a result of the change in resistance.

Current production on uncoated titanium was far lower than on the other materials, and the anode potential was considerably higher (>–150 mV vs. Ag/AgCl at $R = 1000 \Omega$). This may be caused by anodic passivation, which is the formation of a thin metal oxide layer [20]. These titanium oxides are formed when uncoated titanium is in contact with air and they significantly decrease the reaction rate at the electrode. Therefore, uncoated titanium is unsuitable as anode material.

The current density during operation at 100 Ω (Fig. 2A) reached a limit between 2 and 2.5 A/m² at which the anode potential and current density did not become stable. This limit and the instability might be caused by the locally low pH as a result of the accumulation of protons produced by the electrochemically active microorganisms. For each electron, they produce one proton, and when the diffusion of protons to the bulk solution is slow, this can result in a locally low pH, which inhibits the microorganisms. This hypothesis is supported by other research in which it was found that using a concentrated buffer solution, as well as using a buffer solution at high pH, considerably improved MFC performance [6,21].

3.2. Bio-anode polarization curves (dc-voltammetry)

After operation at each resistance, polarization curves were made for the bio-anodes using chronoamperometry, allowing the current and anode potential to stabilize for 120 s for each data point. The result is shown in Fig. 3A–E.

The best performance – highest current densities in combination the lowest anode potentials – were found for the roughened graphite anode in all situations. After operation at a lower resistance ($R = 250 \Omega$), all anodes, except for the uncoated titanium anode, were able to maintain substantially higher current densities during the chronoamperometry measurement (Fig. 3B) compared to before ($R = 1000 \Omega$, Fig. 3A). Fig. 3C, which was made after the unstable operation at 100 Ω , shows that the performance of the anodes decreased compared to Fig. 3B. During the second operation at 250 Ω , the anode potentials were stable, and the polarization curves showed higher current densities again (Fig. 3D). These current densities, however, were lower than obtained before at 250 Ω . After the second operation at 1000 Ω , the current densities showed a further increase (Fig. 3E). The maximum current density decreased in the order roughened graphite > Pt-coated titanium > flat graphite in all situations.

To determine the specific surface area of flat graphite, roughened graphite, and Pt-coated titanium on relevant scales, we have studied the surfaces on the scale of the biofilm (20 $\mu\text{m} \times 20 \mu\text{m}$) and on the scale of a microorganism (2 $\mu\text{m} \times 2 \mu\text{m}$). On the scale of the biofilm, the specific surface area normalized to flat graphite (1.1 $\mu\text{m}^2/\mu\text{m}^2$) decreased in the order Pt-coated titanium (1.9) > roughened graphite (1.2) > flat graphite (1.0). On the scale of a microorganism, the specific surface area normalized to flat graphite (1.1 $\mu\text{m}^2/\mu\text{m}^2$) decreased in the same order: Pt-coated titanium (1.2) > roughened graphite (1.0) = flat graphite (1.0).

As the current density decreased in a different order (roughened graphite > Pt-coated titanium > flat graphite), the surface area is not the single variable explaining the differences in current density for the different materials. Other specific surface properties might have an effect on bacterial attachment and electron transfer and influence the current density in this way. One should also consider that mixed cultures as used in this research have variability by nature, making it more difficult to see the effect of surface area, which differed only a factor 2.

The higher current densities in Fig. 3B as compared to Fig. 3A show that operation at lower resistance improves MFC performance. A lower resistance results in an increased anode potential. At higher anode potentials, the electrochemically active microorganisms can gain more energy from the substrate, as the potential difference between the electron donor (acetate) and the electron acceptor (the anode) is larger. As a consequence, the microorganisms can theoretically gain more energy for growth and higher current can be produced.

3.3. Limiting current density was not caused by mass transfer of the substrate and reflects the maximum biomass activity

A limiting current density was established in the polarization curves, which may indicate mass transfer limitations for the substrate or for the products. Mass transfer limitations for acetate, however, were not likely for two reasons: (i) there was no relationship between the acetate concentration and the observed limiting current density ($R^2 = -2.89$ for linear fit, which indicates that the average is a better representation than the linear fit), and (ii) the observed limiting current density was several times lower than the expected calculated limiting current density (see Section 2), e.g. 4.6 A/m² vs. 39 A/m² at acetate concentration = 6.5×10^{-3} M. The limiting current density was therefore not caused by mass transfer of the substrate and reflected the maximum biomass activity.

Accumulation of product (protons) can also be considered as a mass transfer limitation. Accumulation of products results in a lower overpotential. This mass transfer limitation can be overcome by increasing the overpotential, and does not inhibit or decrease the activity (current density) unless the product is toxic to the microorganisms. Because protons can be toxic to microorganisms, mass transfer limitation of protons could be a reason for the occurrence of a limiting current density. Then, however, the limiting current density in all polarization curves would be the same as the current density determines the rate of proton production. The limiting current was not the same, but different in all situations. So, mass transfer of protons as an explanation for the limiting current density cannot be ruled out for the polarization curve in Fig. 3B which had the highest current density, but is unlikely in the other polarization curves.

We hypothesize that the decrease in current density at higher anode potentials could be caused by damage of enzymes. A higher anode potential might induce damage of the enzymes that are used for electron transfer, as enzymes have a maximum activity at a particular potential [22]. After operation at 100 Ω , however, the polarization curves did show a limiting current, but no maximum (Fig. 3C). At this resistance, the microorganisms were already accustomed to a higher anode potential during the week before the recording of the polarization curves. As a result, the enzymes for electron transfer might not have been damaged at these higher potentials.

3.4. Polarization curves showed high performance, but should be evaluated critically

Most surprisingly, the current densities obtained in these polarization curves with a flat, non-porous electrode were of the same

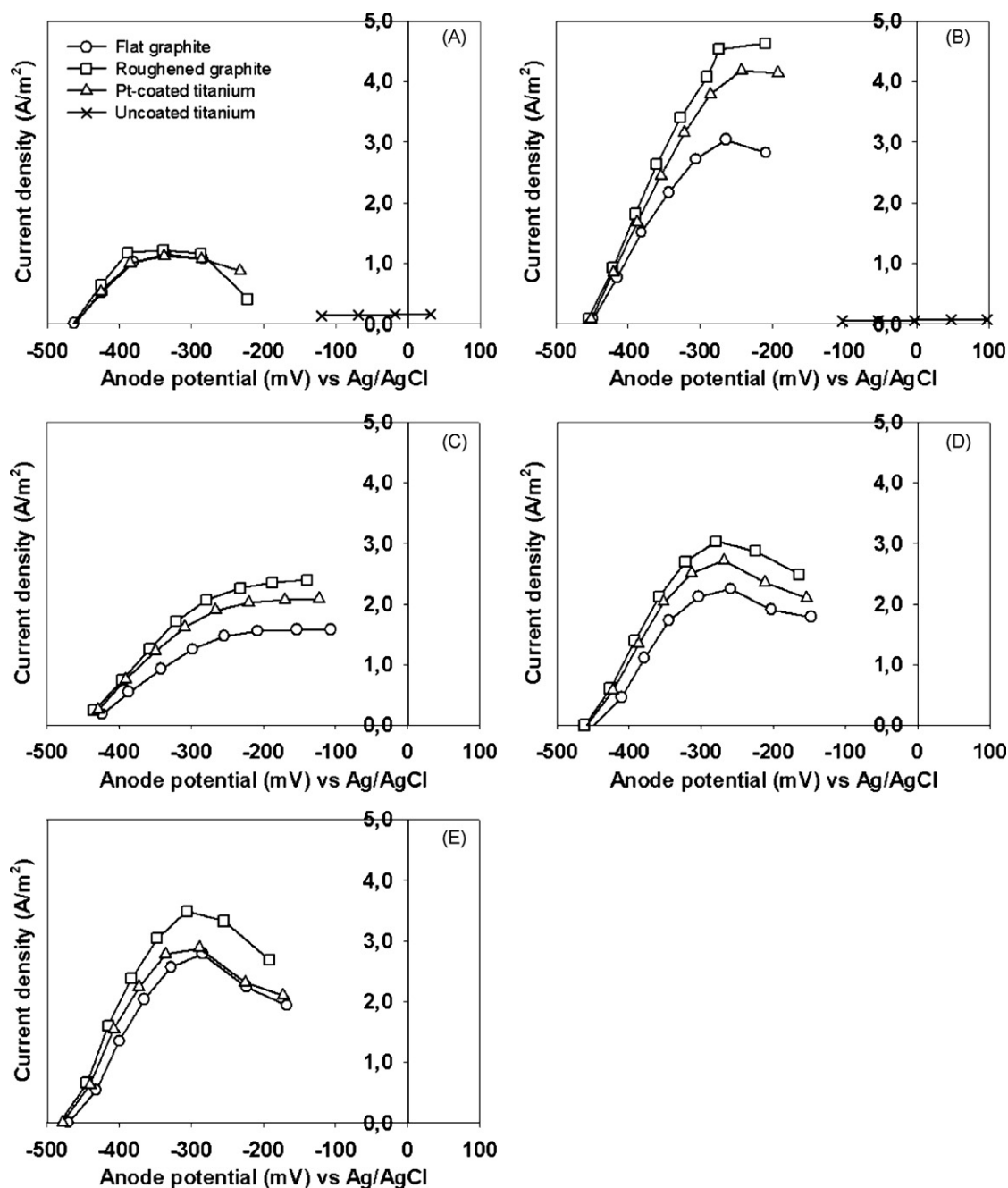


Fig. 3. Polarization curves after operation at (A) 1000 Ω (1st), (B) 250 Ω (1st), (C) 100 Ω, (D) 250 Ω (2nd), and (E) 1000 Ω (2nd).

order of magnitude as the current densities normalized to the projected surface area of porous electrode materials in other studies like graphite felt and graphite cloth, with maximum current densities of, e.g. 4.5 and 8 A/m² [11,6]. This implies that a large part of the surface area of these porous electrode materials was less active, as the same current density can be reached with non-porous electrodes.

Polarization curves are a powerful tool to rapidly evaluate MFC behavior and the development of activity of electrochemically active microorganisms in time [1,23]. Although polarization curves are useful for rapid investigation of MFC behavior, the drawback of polarization curves is that they do not provide information about stable operation in MFCs, and MFC performance is easily overestimated. The maximum current density that was reached in the

polarization curve (Fig. 3C) could not be reached when operated for a longer time period (at lower resistances). Apparently, current densities as high as 4.6 A/m² can be reached on the roughened graphite anode, but due to a limitation in biomass activity it was not possible to sustain higher currents for a longer time period. Besides, large differences were seen in the polarization curves at different times and after operation at different resistances, while the operational condition like temperature, pH, and sufficiently high acetate concentration, were similar in all experiments. The polarization curves that were made after the MFCs were operated for the second time at 250 and 1000 Ω (Fig. 3D and E), were very different from the polarization curves in Fig. 3B (250 Ω, 1st) and A (1000 Ω, 1st), while the current density at these resistances during stable operation (Fig. 2) was the same as before. The lack of stability of the anode potential

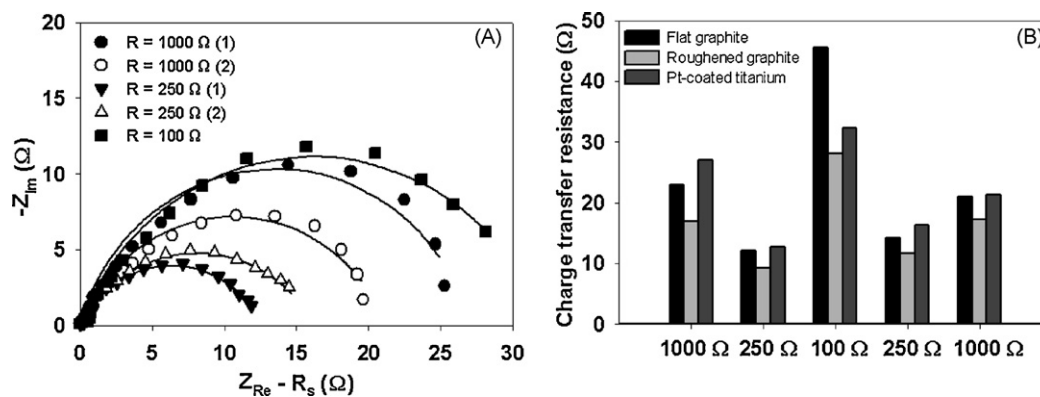


Fig. 4. (A) Nyquist plots for the Pt-coated titanium anode, corrected for the solution resistance. Symbols represent the experimental data, lines represent the fit of these data to the equivalent circuit. (B) Charge transfer resistances as determined from the width of the semicircle in the Nyquist plot.

at higher current densities, and the differences between polarization curves under seemingly similar conditions in this study show that polarization curves of MFCs should be evaluated critically, as was also noted in [24].

3.5. Impedance spectroscopy

The standard geometry of the MFCs enabled reproducible impedance measurements. Nyquist plots for the Pt-coated titanium at the end of each period are shown in Fig. 4A. These Nyquist plots were corrected for the solution resistance to enable comparison. The solution resistances were all in the same range ($12.6 \pm 1.7 \Omega$), which is in accordance with our expectations, as the same MFC configurations with the same electrolytes are used. The absence of a Warburg impedance in the Nyquist plots is another indication of the absence of mass transfer for acetate.

The charge transfer resistance for the anode materials, as determined from the width of the semicircle, was obtained by fitting with the equivalent circuit. The result is shown in Fig. 4B, and supported the difference in performance of the bio-anodes that was found in the polarization curves. The charge transfer resistance for the uncoated titanium anode was $1.8 \times 10^3 \Omega$ (data not shown), which was three orders of magnitude higher than for the other anodes. The roughened graphite anode had the best performance, which is supported by the lowest charge transfer resistance in all measurements. The charge transfer resistance decreased after operation at 250 Ω as compared to operation at 1000 Ω , which might be the result of increased biomass activity. The charge transfer resistance increased considerably after operation at 100 Ω , which is in accordance with the lower current density in the polarization curves (Fig. 3B). The charge transfer resistance decreased again after operation at 250 Ω , which is in accordance with the higher current density in the polarization curves (Fig. 3D). The differences in charge transfer resistance between the materials – like the differences in current density – could not be explained by the differences in specific surface area.

The capacitance, as calculated from the CPE, of the Pt-coated titanium anode was significantly higher ($11.7 \pm 1.1 \text{ mF/cm}^2$, average of the measurements at the 5 resistances) compared to the capacitance of the graphite anodes ($0.72 \pm 0.22 \text{ mF/cm}^2$ for the roughened graphite anode, and $0.23 \pm 0.14 \text{ mF/cm}^2$ for the flat graphite anode). A high capacitance corresponds with a rough electrode surface [25] and thus a high surface area, which is one of the reasons why Pt-coatings are used in fuel cells [26]. This higher capacitance, however, makes the Pt-coated titanium anode less suited for impedance measurements than flat and roughened graphite, as low frequencies are needed to obtain a complete impedance picture. Impedance

measurements at low frequencies have a practical drawback: they require a long measurement time, and it is more difficult to keep the MFC stable during the measurement.

4. Conclusions

With the new experimental setup used in this study, four different anode materials were compared in MFCs under the same conditions. Polarization curves and impedance spectroscopy showed that bio-anode performance normalized to the projected surface area decreased in the order roughened graphite > Pt-coated titanium > flat graphite > uncoated titanium. Uncoated titanium was found to be unsuitable as anode material. For the other three materials, specific surface area was not the single variable explaining the differences in current density for the different materials. All polarization curves showed a clear limiting current. This limit could not be attributed to mass transfer of the substrate and reflected the maximum biomass activity. The high current densities that were recorded by dc-voltammetry, however, could not be maintained in a stable way for a longer period. This shows that polarization curves of MFCs should be evaluated critically.

Acknowledgements

We thank Vinnie de Wilde for technical assistance and design of the experimental setup, Nienke Stein and Wim Borgonje at Wetsus for the MFC design, David Strik and Tom Sleutels for critically reading the manuscript, Mieke Kleijn and Herman van Leeuwen for discussing the results and for the help with the AFM, and Magneto Special Anodes BV for kindly supplying the titanium-based anode materials. This research was funded by SenterNovem, the Dutch governmental agency for sustainability and innovation from the Ministry of Economical Affairs; Besluit Energie Onderzoek Subsidie: Nieuw Energie Onderzoek (grant no: NEOT01015), and supported by Wetsus. Wetsus is funded by the Dutch Ministry of Economic Affairs, the city of Leeuwarden, the Province of Fryslân, the European Union European Regional Development Fund and by the EZ/KOMPAS program of the "Samenwerkingsverband Noord-Nederland".

References

- [1] B.E. Logan, B. Hamelers, R. Rozendal, U. Schröder, J. Keller, S. Freguia, P. Aelterman, W. Verstraete, K. Rabaey, *Environ. Sci. Technol.* 40 (2006) 5181.
- [2] D.R. Lovley, *Nat. Rev. Microbiol.* 4 (2006) 497.
- [3] U. Schröder, *Phys. Chem. Chem. Phys.* 9 (2007) 2619.
- [4] A. ter Heijne, H.V.M. Hamelers, V. De Wilde, R.A. Rozendal, C.J.N. Buisman, *Environ. Sci. Technol.* 40 (2006) 5200.

- [5] K. Rabaey, P. Clauwaert, P. Aelterman, W. Verstraete, *Environ. Sci. Technol.* 39 (2005) 8077.
- [6] S. Cheng, B.E. Logan, *Electrochem. Commun.* 9 (2007) 492.
- [7] Z. He, S.D. Minteer, L.T. Angenent, *Environ. Sci. Technol.* 39 (2005) 5262.
- [8] J. Niessen, U. Schröder, M. Rosenbaum, F. Scholz, *Electrochem. Commun.* 6 (2004) 571.
- [9] U. Schröder, J. Nießen, F. Scholz, *Angew. Chem. Int. Ed.* 42 (2003) 2880.
- [10] M. Rosenbaum, F. Zhao, M. Quaas, H. Wulff, U. Schröder, F. Scholz, *Appl. Catal. B* 74 (2007) 261.
- [11] A. ter Heijne, H.V.M. Hamelers, C.J.N. Buisman, *Environ. Sci. Technol.* 41 (2007) 4130.
- [12] F.P. Van der Zee, R.H.M. Bouwman, D.P.B.T.B. Strik, G. Lettinga, J.A. Field, *Biotechnol. Bioeng.* 75 (2001) 691.
- [13] Z. He, H. Shao, L.T. Angenent, *Biosens. Bioelectron.* 22 (2007) 3252.
- [14] C.H. Hsu, F. Mansfeld, *Corrosion* 57 (2001) 747.
- [15] D.R. Bond, D.R. Lovley, *Appl. Environ. Microbiol.* 69 (2003) 1548.
- [16] G. Reguera, K.P. Nevin, J.S. Nicoll, S.F. Covalla, T.L. Woodard, D.R. Lovley, *Appl. Environ. Microbiol.* 72 (2006) 7345.
- [17] R.E. Hayes, S.T. Kolaczowski, *Chem. Eng. Sci.* 49 (1994) 3587.
- [18] O. Wanner, W. Gujer, *Biotechnol. Bioeng.* 28 (1986) 314.
- [19] A.J. Bard, L.R. Faulkner, *Electrochemical Methods: Fundamentals and Applications*, 2nd ed., John Wiley & Sons, New York, 2001, Ch.1.
- [20] P. Schmuki, *J. Solid State Electrochem.* 6 (2002) 145.
- [21] Y. Fan, H. Hu, H. Liu, *Environ. Sci. Technol.* (2007).
- [22] K.A. Vincent, F.A. Armstrong, *Inorg. Chem.* 44 (2005) 798.
- [23] P. Aelterman, K. Rabaey, H.T. Pham, N. Boon, W. Verstraete, *Environ. Sci. Technol.* 40 (2006) 3388.
- [24] J. Menicucci, H. Beyenal, E. Marsili, R.A. Veluchamy, G. Demir, Z. Lewandowski, *Environ. Sci. Technol.* 40 (2006) 1062.
- [25] Z. He, N. Wagner, S.D. Minteer, L.T. Angenent, *Environ. Sci. Technol.* 40 (2006) 5212.
- [26] D. Thompsett, in: G. Hoogers (Ed.), *Fuel Cell Technology Handbook*, CRC press, 2003, Ch. 6.